THE JOURNAL OF PHYSICAL CHEMISTRY B

Article

Cite This: J. Phys. Chem. B 2018, 122, 4931−4936

pubs.acs.org/JPCB

Monitoring Molecular Transport across Colloidal Membranes

Emilia V. Silletta, Zhe Xu, Mena Youssef, Stefano Sacanna, and Alexej Jerschow*

Department of Chemistry, New York University, 100 Washington Square East, New York, New York 10003, United States

Supporting Information

ABSTRACT: The controlled shaping and surface functionalization of colloidal particles has provided opportunities for the development of new materials and responsive particles. The possibility of creating hollow particles with semipermeable walls allows modulating molecular transport properties on colloidal length scales. While shapes and sizes can typically be observed by optical means, the underlying chemical and physical properties are often invisible. Here, we present measurements of cross-membrane transport via pulsed field gradient NMR in packings of hollow colloidal particles. The work is conducted using a systematic selection of particle sizes, wall permeabilities, and osmotic pressures and allows tracking organic molecules as well as ions. It is also shown that, while direct transport of molecules can be measured, indirect markers can be obtained for invisible species via the osmotic pressure as well. The cross-membrane transport information is important for applications in nanoconfinement, nanofiltration, nanodelivery, or nanoreactor devices.

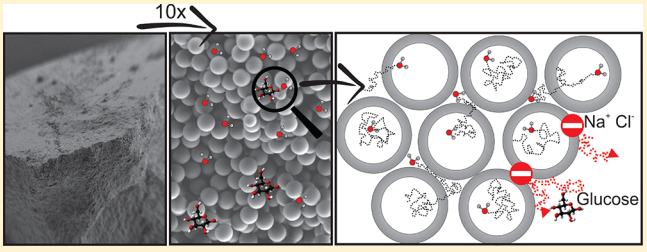

INTRODUCTION

Colloids are exceptionally versatile materials of broad relevance to many areas of modern science and industry.[1−4] Many biological and industrial processes rely fundamentally on the properties of colloidal suspensions. The unique behavior of colloids is rooted in the high surface area and soft interaction potentials that have the magnitude of thermal fluctuations. Colloidal interactions can be tuned by chemically modifying the particle surfaces, for example, via the addition of polymer brushes, charged surface groups, and even DNA strands. The result is a suspension of particles engineered to display a wide range of behaviors, from simple hard spheres[5] to atomic analogues that interact via a complex mix of directional and selective bonds.[6] These colloidal fluids can self-assemble into elaborate three-dimensional architectures and undergo phase transitions that are similar to those observed in atomic and molecular systems.[5] The generation of colloidal membrane particles with hollow interiors opens a pathway toward exploiting their permeability properties in terms of delivering a "payload" to a point of interest, to act as nanofiltration agents for molecules, ions, and perhaps even viruses or bacteria, or to produce nanoreactor environments.[7−15]

While colloid and emulsion sizes can be determined reliably by optical means, such as using light scattering or confocal microscopy,[16] their chemical properties often remain invisible to these methods. In particular, cross-membrane transport and the relative distribution of molecules between intra- and interparticle space is difficult to measure without a significant perturbation of the system. Fluorescence imaging is a powerful technique for monitoring the permeability of capsules,[17] but a fluorescent probe is needed and its presence can alter the dynamics and limit the functional chemical space. In this work, we study molecular cross-membrane transport in packings of hollow colloidal shell particles with time-dependent NMR diffusometry.

Pulsed field gradient (PFG) NMR has been used, for example, to study the permeability of human erythrocytes,[18] the transport through Nafion mesoporous membranes,[19] or the transference numbers in ionic liquids.[20] Although quasi-elastic neutron scattering (QENS) can be used to probe molecular-level dynamic information on scales ranging from Å to nm, PFG-NMR is sensitive to dynamics on length scales of a few μm to mm, is chemically specific, and is a more easily accessible method.[21−23] Time-dependent diffusion measurements have been used to study porous media, giving access to information such as the surface-to-volume (S/V) ratio, tortuosity/porosity,[24] and permeability.[25]

Diffusion experiments are widely used in heterogeneous and multicompartment systems, such as, for example, in porous media or tissues.[26,27] Generally, two types of models are used to interpret the data. The first type uses well-defined assumptions about the system geometry, which makes the application and interpretation straightforward. This model has been applied to several different systems, for example, porous media,[26] packed erythrocytes,[27] and bovine optic nerve,[28] among others. On the other hand, the second approach is not concerned with the geometry and treats the system as an abstract multisite exchange model. The two-site exchange model was first applied by McConnell[29] to determine cell membrane permeabilities, and later on, Kärger[30,31] and Andrasko[18] studied the two-compartment exchange to analyze diffusion-weighted imaging, using the so-called Kärger model.[30] The standard diffusion PFG

Received: February 15, 2018
Revised: March 22, 2018
Published: April 17, 2018

DOI: 10.1021/acs.jpcb.8b01638
J. Phys. Chem. B 2018, 122, 4931−4936

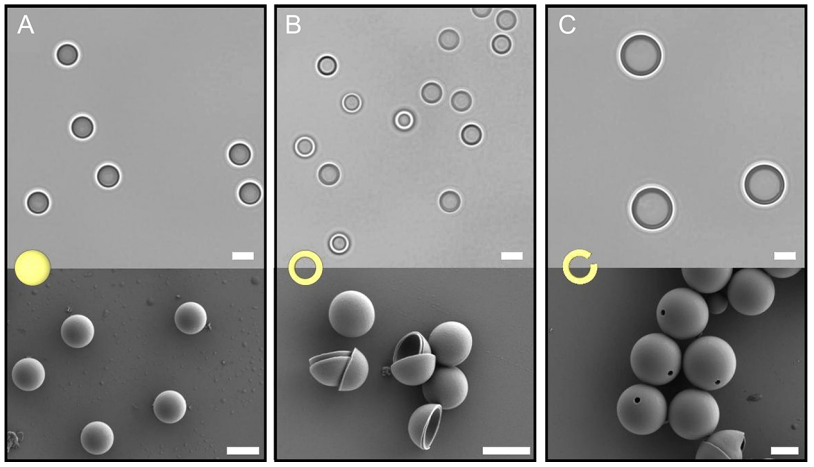

Figure 1. Bright-field (top) and electron (bottom) microscopy images showing the three colloidal model systems used in this study. (A) Solid TPM spheres, (B) hollow TPM particles with a wall thickness of approximately 100 nm, and (C) hollow TPM particles with a hole in the surface. All scale bars are 3 μm. The outer diameters are as follows: solid TPM spheres, d = 2.9 ± 0.1 μm; hollow TPM particles, d = 2.7 ± 0.2 μm; hollow TPM particles with a hole (PS inclusions removed), d = 5.6 ± 0.5 μm with the hole diameter being approximately 650 nm.

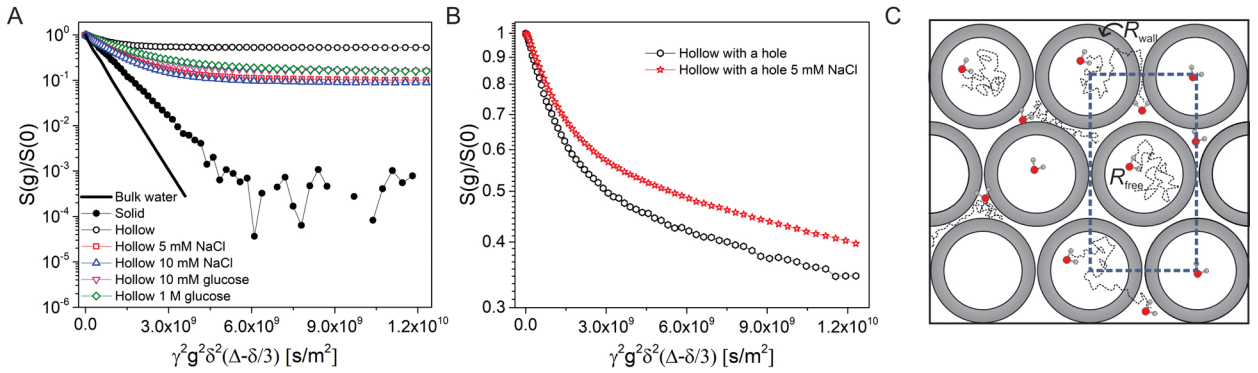

Figure 2. (A) Normalized signal attenuation in a PFGSE experiment for 50 ms of diffusion time for solid and hollow colloids. The diffusion dynamics in solid particles can be described with only one diffusion coefficient, while two are necessary for hollow colloids. The diameter of solid particles is 2.9 μm, while for hollow particles it is 2.7 μm. The decay of the signal for bulk water is added for comparison (solid black line). (B) The diffusion dynamics in particles with a hole shows a biexponential decay. For all particles, the presence of NaCl or glucose changes the diffusion coefficients as well as their relative contributions. The diameter of the particles with a hole shown in part B is 5.6 μm. (C) Scheme of a 2D slice of the 3D packing geometry used in the Monte Carlo simulations for hollow colloids. Water molecules can diffuse inside the particles or in the interparticle space. White space represents the allowed regions for molecules to diffuse freely, and the gray region represents the polymeric shell. The box represents the unit cell used for the MC simulations with periodic boundary conditions.

sequence can also be applied in two dimensions, where $D-D$ maps are obtained and, varying the storage time, the exchange between different environments can be calculated.[32,33] This method is useful for many applications, but it is time-demanding because a 2D data set has to be acquired at each storage time. Furthermore, diffusion experiments can be combined with relaxation experiments and exchange times can be determined, for example, in a system of phenol molecules in a colloidal dispersion of hollow polymeric capsules.[34] In that case, the phenol is binding to the capsule wall rather than encapsulated in the interior.

Here, we use time-dependent NMR diffusometry to study multicompartment colloidal systems and probe the molecular transport across the colloidal membranes noninvasively. We make no a priori assumptions about the diffusion and relaxation parameters. From the time-dependent diffusion, we obtain not only the exchange dynamics but also the S/V ratio. Furthermore, the inner diameter of the void space and the wall thickness can be inferred through measurements of the S/V ratio in the two compartments. A Monte Carlo (MC) computational model is used to reproduce the experimental results, to provide estimates of the membrane permeability, and to provide further insights into the membrane permeation process.

EXPERIMENTAL SECTION

Three different systems were used to study the dynamics: (i) solid 3-(trimethoxysilyl)propyl methacrylate (TPM) polymer spheres, (ii) hollow TPM particles of different sizes, and (iii) hollow TPM particles with a hole on the surface (Figure 1).

The colloidal model systems are synthesized by emulsion templating[35] using monodispersed emulsions of 3-(trimethoxysilyl)propyl methacrylate (TPM) prepared similar to the procedure described in ref 36. The process involves droplet nucleation and growth in water, TPM cross-linking, and controlled polymerization via radical or UV initiation. The size ranges can be adjusted by the exact conditions, and size standard deviations are in the range 4–9% (see Figure 1). The procedure and conditions are summarized in the Supporting Information. Colloidal packings were prepared by centrifuging,

DOI: 10.1021/acs.jpcb.8b01638
J. Phys. Chem. B 2018, 122, 4931−4936

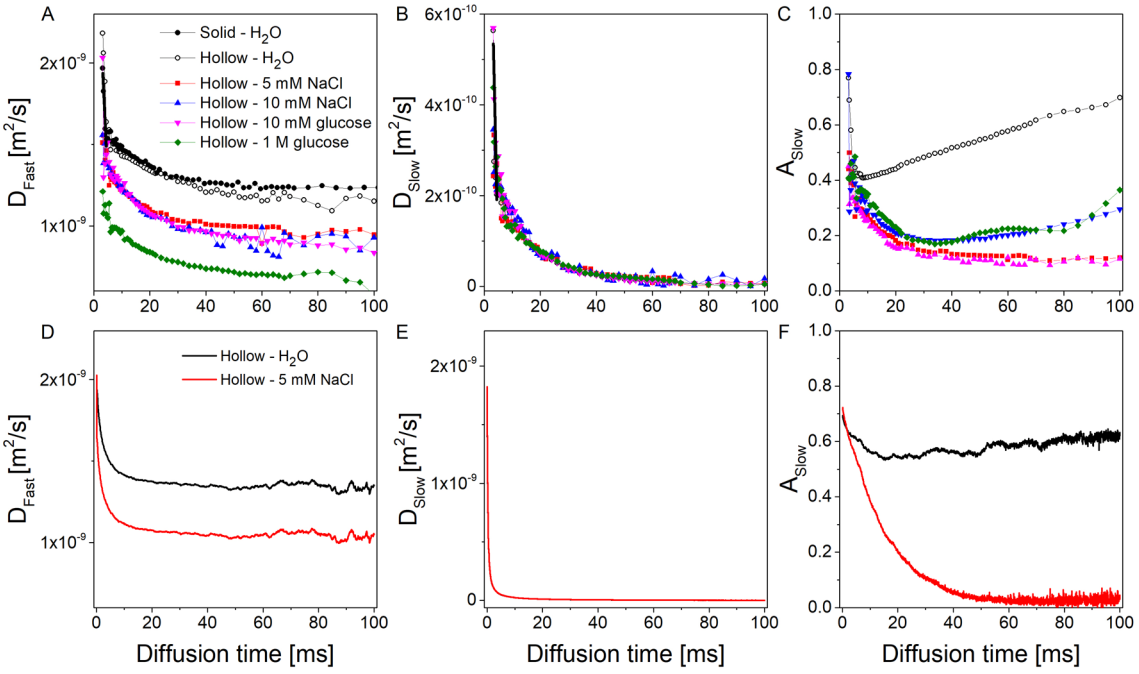

Figure 3. (A) Fast diffusion coefficient as a function of diffusion time for hollow particles (outer diameter of 2.7 μm) imbibed in pure H_2O, 5 mM NaCl, 10 mM NaCl, 10 mM glucose, and 1 M glucose. Closed symbols show the data from monoexponential fitting for the curves acquired for solid particles with a diameter of 2.9 μm for comparison. (B) Slow diffusion coefficient as a function of diffusion time for hollow colloids. (C) The relative contribution of the slow diffusion component. MC simulations showing (D) fast and (E) slow diffusion coefficients in hollow colloids and (F) the relative contribution of the slow diffusion component. Black and solid lines show the results from simulations mimicking the experimental samples imbibed in pure water and 5 mM NaCl, respectively. The corresponding self-diffusion coefficients and the relaxation effects for each solution were used.

and packings were checked by NMR relaxation measurements to diagnose changes in surface-to-volume ratios. The packing procedure, packing density, uniformity, and degree of crystallinity were examined by SEM (Figure S1).

The NMR experiments were carried out on a Bruker Avance I spectrometer (Bruker, MA, USA) operating at 400.13 MHz for ^{1}H. Diffusion experiments were collected with a Bruker Micro2.5 gradient assembly with a maximum gradient intensity of 1 T/m. The applied gradients were calibrated using water. A PFGSE sequence was used for the diffusion experiments where the diffusion time was varied from 2 to 100 ms and the duration of the gradient was set to 1 ms. The temperature was controlled at 24 °C for all measurements. Diffusion coefficients were determined by fitting PFGSE experimental curves to a mono- or biexponential function using MATLAB and determining the amplitudes (A_i) and diffusion coefficients (D_i) of the components.

RESULTS AND DISCUSSION

The signal attenuation curve for a PFGSE experiment at a fixed diffusion time (50 ms) with increasing gradient strengths is shown in Figure 2 for a range of particle samples. The signal attenuation for solid particles (black closed circles in Figure 2A) shows a monoexponential decay over a large range until the sensitivity limit is reached. The monoexponential decay for these solid spheres indicates that the packing is sufficiently uniform, and no significant restricted diffusion behavior is seen, which implies that the interparticle space is sufficiently connected. The decay is less steep than that for bulk water (solid black line) because of the tortuosity in the colloid sample. The same experiment performed on packings of hollow particles (black open circles in Figure 2A) shows a markedly different behavior, namely, clear evidence of restricted diffusion, which can be attributed to the volume fraction inside the particles. It is thus reasonable to assume that the curve consists of two components, one with slow diffusion (volume inside the particles or restricted diffusion fraction) and one with fast diffusion (interparticle space). Marked changes are seen when the particles are suspended in NaCl or glucose solutions where the self-diffusion coefficient varies (in line with the variation in bulk solutions, as seen in Table S1). Figure 2B demonstrates the behavior of the hollow TPM particles with the hole on the surface, showing clear evidence of compartment exchange. Some restriction is seen, as expected, because of the relative scales of the hole in relationship to the particle size (see Figure 1C). The probability of leaving the particle simply based on relative hole size would be given by 0.0034. In Figure 2C, the 2D scheme of the hollow particle system can be seen, where the box represents the unit cell used for the MC simulations discussed below.

In order to further analyze the restricted diffusion behavior and molecular interchange between compartments, time-dependent diffusion measurements were carried out. In Figure 3, the time-dependent diffusion coefficients for both the fast and slow components as well as the fraction of the slow diffusion component (A_{slow}) are plotted for solid and hollow particles in different aqueous solutions. Figure 3A shows that the fast component of the diffusion can be assigned to the interparticle space, since the diffusion curve of the interparticle space from solid particle samples agrees with the curve of the fast diffusion compartment in hollow particles imbibed in pure water. Furthermore, one can deduce from this result that the packing behavior of the different particles is very similar because both diffusion coefficients appear to reach a similar

DOI: 10.1021/acs.jpcb.8b01638
J. Phys. Chem. B 2018, 122, 4931−4936

plateau value (solid and open black symbols). At long diffusion times, D_{eff}/D_0 tends to a value of $1/\alpha$, where α is the tortuosity. In simple model systems (for example, spherical bead packs), α can be calculated as $\phi^{-1/2}$, where ϕ is the volume fraction of the pore space, i.e., the porosity.[37] For a closely packed system, the porosity is $\phi = 0.259$. The porosities calculated from the data in Figure 3A are $\phi = 0.28$ for hollow particles and $\phi = 0.33$ for solid spheres. Some deviations from the close packing values seen in the SEM images in Figure S1 would explain the somewhat larger measured porosity values.

The limiting value of the fast diffusion coefficient is still larger than the fastest component of the slow diffusion values obtained (Figure 3B) by a factor of 2. The slow diffusion component for hollow colloids further shows a more rapid decrease, thus indicating a strong restriction for a large fraction of particles. The behavior of the fraction of the slow components is shown in Figure 3C as a function of diffusion time (the fast diffusion fraction would simply be $1 - A_{Slow}$). One can see that after initially big changes (over ~5 ms) the slow component fraction appears to rise. This effect can be attributed in part to differential relaxation effects, which will be further explored below.

From the time-dependent diffusion measurements, information about the spatial restriction can be obtained via[26]

$$\frac{D_{eff}(t)}{D_0} = 1 - \frac{4\sqrt{D_0 t}}{9\sqrt{\pi}}\frac{S}{V_p} = ax + b$$

Assuming a spherical internal volume, such is the case for intraparticle void space, the inner diameter of the hollow spheres can be calculated via $d = \frac{4}{9\sqrt{\pi}}\frac{6}{a}$, where a is the slope of the linear curve for D_{Slow} (black line in Figure 3B), giving, as a result, $d = 2.6 \pm 0.2$ μm. Knowing that the diameter of the sphere is 2.9 μm, the wall thickness can be estimated as 0.15 μm, which is in agreement with the SEM pictures. For the fitting at short diffusion times from D_{Fast}, the interparticle S/V ratios can be determined for both solid and hollow colloids, as shown in Figure 3A (the black line corresponds to the fitting of the hollow colloid data). For solid TPM spheres, $S/V_{sol} = 1.95$ μm^{-1}, while $S/V_{hol} = 2.1$ μm^{-1} for hollow TPM particles. The theoretical value for a close-packed system of spheres with that diameter is $S/V_{cp} = 2.7$ μm^{-1}. The lower experimental values are consistent with the porosity calculations, together with the SEM images, showing a crystalline but not close-packed arrangement.

As a next step, we examined the ability to assess the penetration of salt ions and glucose through the shell wall and the role of osmotic pressure on the diffusion dynamics. In Figure 3A, it is clearly observed that the fast diffusion coefficients vary depending on the type of solution used for imbibing. Higher salt concentrations and higher glucose concentrations lead to smaller diffusion coefficients in the interparticle space (D_{Fast}, Figure 3A). The ratios of the diffusion coefficients correspond to the expected ratios obtained from the self-diffusion coefficients measured in the respective pure solutions (Table S1). Figure 3B, on the other hand, shows that the restricted diffusion component is almost the same for all samples. This finding clearly indicates that neither salt ions nor glucose enter the hollow particles. Direct measurements of glucose diffusion support this finding (Figures S2 and S3A). Another important distinction is that the fraction of the restricted diffusion component (Figure 3C) is much lower than that in the pure water results (open circles). This effect is not as strong for glucose samples, and overall, it does not appear to change much over the examined concentration range. At a higher salt concentration, such as 1 M NaCl, the slow diffusion fraction is almost constant over the whole observation time because of the high osmotic pressure that compresses the particles, thus leading to a bigger space for molecules in the interparticle pores (data not shown).

As a further control experiment, hollow particles with a hole on the surface were examined (Figure S3B), and the slow diffusion coefficient is shown in two different solutions: pure water and 5 mM NaCl solution. Since the hole is sufficiently large to allow for permeation of salt ions but still retain diffusion restriction, biexponential diffusion is again observed (Figure 2B). It is now clearly seen that the slow diffusion component shows the presence of salt ions, since the diffusion coefficient changes with the change of imbibing solution (as opposed to the case shown in Figure 3B). Therefore, in combination with the results from Figure 3B, we can conclude that salt ions do not enter the inside compartment when there is no hole in the surface. In Figure S4, the complete fast and slow diffusion time-dependent results are shown for the particles with the hole on the surface. In addition, the comparison with the hollow particles with the same diameter is shown.

MC simulations can now be used to model the observed effects in order to extract wall permeability values. Parts D−F of Figure 3 show the MC simulations for hollow colloids. For these calculations, 10^5 trajectories were considered where the maximum diffusion time is 100 ms and the length of a single step j_l is 10 nm. The simulation details are summarized in the Supporting Information. Both diffusion curves start from the same value because, at very short times, the diffusion can be considered to be free (Figure 3D,E). This point cannot be reached experimentally because of the longer minimum diffusion time required. In Figure 3F, the contributions for slow diffusion are calculated.

It is important to note that the relative amplitudes shown in Figure 3C,F depend not only on diffusion but also on the differential effect of relaxation between the compartments (see also the unnormalized decays in Figure S5). For samples with NaCl or glucose, the signal arising from molecules inside the particles decays much faster than when pure water is used as a solvent (a factor of almost 4). To reproduce this effect, the MC model was modified to assign a particular decay for every wall crossing (R_{wall}) and a different one for wall reflection. The black line in Figure 3D−F shows the result considering the self-diffusion coefficient for pure water (Table S1) and the corresponding relaxation found experimentally (Figure S5), while the red line shows the MC results using the diffusion coefficient for 5 mM NaCl solution with the respective relaxation effect. By comparing these simulations with the experimental results in Figure 3, it can therefore be concluded that the factor that dominates the longer-term relaxation behavior is the molecular wall traversal. This parameter could be of further use to determine the effective wall thickness. It is also found that, when the osmotic pressure is high, the slow diffusion component is more strongly affected by relaxation.

Finally, from MC simulations, the permeability of the TPM shell can be estimated. The permeability value is calculated from eq 1 in the Supporting Information, where it is shown that the permeability with respect to a particular molecule is a function of both the rate of diffusion toward the membrane (D)

DOI: 10.1021/acs.jpcb.8b01638
J. Phys. Chem. B 2018, 122, 4931−4936

and the rate of exchange across it (probability p in MC).[38] To reproduce experimental results, the probability of exchange p was chosen as 10^{-4} in the simulations of pure water, from which a wall permeability of $P = 2.30 \times 10^{-5}$ m/s is obtained. Details on the MC simulations are provided in the Supporting Information.

CONCLUSIONS

In conclusion, we have demonstrated here that NMR diffusometry allows monitoring inter- and intraparticle dynamics and molecular transport across colloidal membranes. Time-dependent diffusion experiments of particles with different properties and in different solutions indicated that both direct and indirect measurements allowed molecular penetration properties into the interior particle space to be determined. Monte Carlo simulations reproduced the experimental findings and provided access to the membrane permeability factor and to relaxation parameters during wall permeation. These studies address the need to examine molecular-level properties of colloidal shell particles, which could be used for nanofiltration, as nanoreactors, or as molecular delivery vehicles.

ASSOCIATED CONTENT

Supporting Information

The Supporting Information is available free of charge on the ACS Publications website at DOI: 10.1021/acs.jpcb.8b01638.

Additional text and Figures S1–S5 related to the synthesis of colloidal particles, colloidal packing, free water self-diffusion in different solutions, and Monte Carlo simulations (PDF)

AUTHOR INFORMATION

Corresponding Author

*E-mail: alexej.jerschow@nyu.edu.

ORCID

Emilia V. Silletta: 0000-0003-2856-2112

Stefano Sacanna: 0000-0002-8399-3524

Alexej Jerschow: 0000-0003-1521-9219

Notes

The authors declare no competing financial interest.

ACKNOWLEDGMENTS

The work was supported primarily by the MRSEC Program of the National Science Foundation under Award No. DMR-1420073 and partially by Award No. CHE 1710046. The Zeiss Merlin field emission SEM was acquired through the support of the NSF under Award No. DMR-0923251.

REFERENCES

(1) Wang, Y.; Wang, Y.; Zheng, X.; Ducrot, E.; Yodh, J. S.; Weck, M.; Pine, D. J. Crystallization of DNA-coated colloids. *Nat. Commun.* **2015**, *6*, 7253.

(2) Weeks, E. R.; Crocker, J. C.; Levitt, A. C.; Schofield, A.; Weitz, D. A. Three-Dimensional Direct Imaging of Structural Relaxation Near the Colloidal Glass Transition. *Science* **2000**, *287*, 627–631.

(3) Nelson, D. R. Toward a Tetravalent Chemistry of Colloids. *Nano Lett.* **2002**, *2* (10), 1125–1129.

(4) Glotzer, S. C.; Solomon, M. J. Anisotropy of Building Blocks and their Assembly into Complex Structures. *Nat. Mater.* **2007**, *6*, 557–562.

(5) Pusey, P. N.; van Megan, W. Phase Behaviour of Concentrated Suspensions of Nearly Hard Colloidal Spheres. *Nature* **1986**, *320*, 340–342.

(6) Wang, Y.; Wang, Y.; Breed, D. R.; Manoharan, V. N.; Feng, L.; Hollingsworth, A. D.; Weck, M.; Pine, D. J. Colloids with Valence and Specific Directional Bonding. *Nature* **2012**, *491* (7422), 51–55.

(7) Ji, L.; Liang, G.; Si, Y.; Qiao, W.; Zhang, Y.; Zhu, A.; Qiu, D. Engineering Colloids with Narrow Size Distribution in a Three Dimensional Ordered Macroporous Carbon Microreactor. *Mater. Lett.* **2017**, *190*, 1–4.

(8) Dickhout, J. M.; Moreno, J.; Biesheuvel, P. M.; Boels, L.; Lammertink, R. G. H.; de Vos, W. M. Produced Water Treatment by Membranes: A Review from a Colloidal Perspective. *J. Colloid Interface Sci.* **2017**, *487*, 523–534.

(9) Sanchez-Rodriguez, S. P.; Moran-Garcia Adel, C.; Bolonduro, O.; Dordick, J. S.; Bustos-Jaimes, I. Enhanced Assembly and Colloidal Stabilization of Primate Erythroparvovirus 1 Virus-like Particles for Improved Surface Engineering. *Acta Biomater.* **2016**, *35*, 206–214.

(10) Rusen, E.; Mocanu, A.; Nistor, L. C.; Dinescu, A.; Calinescu, I.; Mustatea, G.; Voicu, S. I.; Andronescu, C.; Diacon, A. Design of Antimicrobial Membrane Based on Polymer Colloids/Multiwall Carbon Nanotubes Hybrid Material with Silver Nanoparticles. *ACS Appl. Mater. Interfaces* **2014**, *6* (20), 17384–17393.

(11) Zhou, J. L.; Lui, R.; Wilding, A.; Hibberd, A. Sorption of Selected Endocrine Disrupting Chemicals to Different Aquatic Colloids. *Environ. Sci. Technol.* **2007**, *41*, 206–213.

(12) Wegmann, M.; Michen, B.; Luxbacher, T.; Fritsch, J.; Graule, T. Modification of Ceramic Microfilters with Colloidal Zirconia to Promote the Adsorption of Viruses from Water. *Water Res.* **2008**, *42* (6–7), 1726–1734.

(13) Uskokovic, V.; Drofenik, M. Reverse Micelles: Inert Nanoreactors or Physico-Chemically Active Guides of the Capped Reactions. *Adv. Colloid Interface Sci.* **2007**, *133* (1), 23–34.

(14) Caruso, F.; Caruso, R. A.; Möhwald, H. Nanoengineering of Inorganics and Hybrid Hollow Spheres by Colloidal Templating. *Science* **1998**, *282*, 1111–1114.

(15) Caruso, F.; Trau, D.; Möhwald, H.; Renneberg, R. Enzyme Encapsulation in Layer-by-Layer Engineered Polymer Multilayer Capsules. *Langmuir* **2000**, *16*, 1485–1488.

(16) Kodger, T. E.; Guerra, R. E.; Sprakel, J. Precise Colloids with Tunable Interactions for Confocal Microscopy. *Sci. Rep.* **2015**, *5*, 14635.

(17) Ma, Y.; Dong, W. F.; Hempenius, M. A.; Möhwald, H.; Vancso, G. J. Redox-Controlled Molecular Permeability of Composite-Wall Microcapsules. *Nat. Mater.* **2006**, *5* (9), 724–729.

(18) Andrasko, J. Water Diffusion Permeability of Human Erythrocytes Studied by a Pulsed Gradient NMR Technique. *Biochim. Biophys. Acta, Gen. Subj.* **1976**, *428*, 304–311.

(19) Yang, H.; Zhang, J.; Li, J.; Jiang, S. P.; Forsyth, M.; Zhu, H. Proton Transport in Hierarchical-Structured Nafion Membranes: A NMR Study. *J. Phys. Chem. Lett.* **2017**, *8* (15), 3624–3629.

(20) Hoarfrost, M. L.; Tyagi, M.; Segalman, R. A.; Reimer, J. A. Proton Hopping and Long-Range Transport in the Protic Ionic Liquid [Im][TFSI], Probed by Pulsed-Field Gradient NMR and Quasi-Elastic Neutron Scattering. *J. Phys. Chem. B* **2012**, *116* (28), 8201–8209.

(21) Berrod, Q.; Lyonnard, S.; Guillermo, A.; Ollivier, J.; Frick, B.; Manseri, A.; Améduri, B.; Gébel, G. Nanostructure and Transport Properties of Proton Conducting Self-Assembled Perfluorinated Surfactants: A Bottom-Up Approach toward PFSA Fuel Cell Membranes. *Macromolecules* **2015**, *48* (17), 6166–6176.

(22) Perrin, J. C.; Lyonnard, S.; Volino, F. Quasielastic Neutron Scattering Study of Water Dynamics in Hydrated Nafion Membranes. *J. Phys. Chem. C* **2007**, *111*, 3393–3404.

(23) Berrod, Q.; Hanot, S.; Guillermo, A.; Mossa, S.; Lyonnard, S. Water Sub-Diffusion in Membranes for Fuel Cells. *Sci. Rep.* **2017**, *7* (1), 8326.

(24) Callaghan, P. T. *Translational Dynamics and Magnetic Resonance: Principles of Pulsed Gradient Spin Echo NMR*; 2011.

DOI: 10.1021/acs.jpcb.8b01638
J. Phys. Chem. B 2018, 122, 4931–4936

(25) Latour, L. L.; Mitra, P. P.; Kleinberg, R. L.; Sotak, C. H. Time-Dependent Diffusion Coefficient of Fluids in Porous Media as a Probe of Surface-to-Volume Ratio. *J. Magn. Reson., Ser. A* **1993**, *101*, 342−346.
(26) Mitra, P. P.; Sen, P. N.; Schwartz, L. M.; Le Doussal, P. Diffusion Propagator as a Probe of the Structure of Porous Media. *Phys. Rev. Lett.* **1992**, *68* (24), 3555−3558.
(27) Latour, L. L.; Svoboda, K.; Mitra, P. P.; Sotak, C. H. Time-Dependent Diffusion of Water in a Biological Model System. *Proc. Natl. Acad. Sci. U. S. A.* **1994**, *91*, 1229−1233.
(28) Stanisz, G. J.; Szafer, A.; Wright, G. A.; Henkelman, R. M. An Analytical Model of Restricted Diffusion in Bovine Optic Nerve. *Magn. Reson. Med.* **1997**, *37*, 103−111.
(29) McConnell, H. M. Reaction Rates by Nuclear Magnetic Resonance. *J. Chem. Phys.* **1958**, *28* (3), 430−431.
(30) Kärger, J. NMR Self-Diffusion Studies in Heterogeneous Systems. *Adv. Colloid Interface Sci.* **1985**, *23*, 129−148.
(31) Kärger, J.; Pfeifer, H.; Heink, W. Principles and Applications of Self-Diffusion Measurements by Nuclear Magnetic Resonance. *Adv. Magn. Opt. Reson.* **1988**, *12*, 1−89.
(32) Callaghan, P. T.; Furo, I. Diffusion-Diffusion Correlation and Exchange as a Signature for Local Order and Dynamics. *J. Chem. Phys.* **2004**, *120* (8), 4032−4038.
(33) Qiao, Y.; Galvosas, P.; Adalsteinsson, T.; Schonhoff, M.; Callaghan, P. T. Diffusion Exchange NMR Spectroscopic Study of Dextran Exchange Through Polyelectrolyte Multilayer Capsules. *J. Chem. Phys.* **2005**, *122* (21), 214912.
(34) Choudhury, R. P.; Schonhoff, M. Pulsed Field Gradient NMR Study of Phenol Binding and Exchange in Dispersions of Hollow Polyelectrolyte Capsules. *J. Chem. Phys.* **2007**, *127* (23), 234702.
(35) Zoldesi, C. I.; Imhof, A. Synthesis of Monodisperse Colloidal Spheres, Capsules, and Microballoons by Emulsion Templating. *Adv. Mater.* **2005**, *17* (7), 924−928.
(36) van der Wel, C.; Bhan, R. K.; Verweij, R. W.; Frijters, H. C.; Gong, Z.; Hollingsworth, A. D.; Sacanna, S.; Kraft, D. J. Preparation of Colloidal Organosilica Spheres through Spontaneous Emulsification. *Langmuir* **2017**, *33* (33), 8174−8180.
(37) Sen, P. N.; Schwartz, L. M.; Mitra, P. P.; Halperin, B. I. Surface Relaxation and the Long-Time Diffusion Coefficient in Porous Media: Periodic Geometries. *Phys. Rev. B: Condens. Matter Mater. Phys.* **1994**, *49* (1), 215−225.
(38) Regan, D. G.; Kutchel, P. W. Mean Residence Time of Molecules Diffusing in a Cell Bounded by a Semi-Permeable Membrane: Monte Carlo Simulations and an Expression Relating Membrane Transition Probability to Permeability. *Eur. Biophys. J.* **2000**, *29*, 221−227.

DOI: 10.1021/acs.jpcb.8b01638
J. Phys. Chem. B 2018, 122, 4931−4936